catalysts

MDPI

Article

Highly Selective Transformation of CO_2 + H_2 into Para-Xylene via a Bifunctional Catalyst Composed of Cr_2O_3 and Twin-Structured ZSM-5 Zeolite

Shiyuan Lin [1], Ruosong He [1], Wenhang Wang [1,2], Yang Wang [1,2,*], Yongqiang Gu [1,2], Qiang Liu [3] and Mingbo Wu [1,*]

[1] College of New Energy, State Key Laboratory of Heavy Oil Processing, China University of Petroleum (East China), Qingdao 266580, China; z20150006@s.upc.edu.cn (S.L.); s21150001@s.upc.edu.cn (R.H.); d2078101@ems.u-toyama.ac.jp (W.W.); d2178102@ems.u-toyama.ac.jp (Y.G.)
[2] Department of Applied Chemistry, Graduate School of Engineering, University of Toyama, Gofuku 3190, Toyama 930-8555, Japan
[3] National Engineering Research Center of Coal Gasification and Coal-Based Advanced Materials, Shandong Energy Group Co., Ltd., Jinan 250014, China; sdqliu@sohu.com
* Correspondence: wangyang@upc.edu.cn (Y.W.); wumb@upc.edu.cn (M.W.)

Abstract: The abundant C1 source CO_2 can be utilized to produce value-added chemicals through hydrogenation technology. A bifunctional catalyst consisting of reducible metal oxide Cr_2O_3 and acidic zeolite ZSM-5 was designed for the direct conversion of CO_2 + H_2 into valuable aromatics, especially para-xylene (PX), via the methanol-mediated pathway. The twin structure of ZSM-5 (ZSM-5^T), with sinusoidal channels that are predominantly exposed to the external surface, enhances the possibility of the transformation of methanol into PX due to the favorable diffusion dynamic of PX in the sinusoidal channels. Via the bifunctional catalyst Cr_2O_3&ZSM-5^T, a PX selectivity of 28.7% and PX space-time yield (STY) of 2.5 g_{CH2} h^{-1} $kg_{cat}{}^{-1}$ are achieved at a CO_2 conversion rate of 16.5%. Furthermore, we rationally modify the ZSM-5^T zeolite via Cu species doping and amorphous SiO_2 shell coating (Cu-ZSM-5^T@SiO_2). After combining with the Cr_2O_3 catalytic component, the CO_2 conversion (18.4%) and PX selectivity (33.8%) are increased to some extent, which systematically increases the STY of PX to 3.0 g_{CH2} h^{-1} $kg_{cat}{}^{-1}$. The physicochemical property of the acidic zeolite and the corresponding structure-function relationship in enhancing the PX productivity are discovered. Our work provides a novel catalyst design idea to boost PX synthesis performance from CO_2 hydrogenation.

Keywords: CO_2 hydrogenation; bifunctional catalysts; para-xylene; H-ZSM-5 zeolites

check for updates

Citation: Lin, S.; He, R.; Wang, W.; Wang, Y.; Gu, Y.; Liu, Q.; Wu, M. Highly Selective Transformation of CO_2 + H_2 into Para-Xylene via a Bifunctional Catalyst Composed of Cr_2O_3 and Twin-Structured ZSM-5 Zeolite. *Catalysts* **2023**, *13*, 1080. https://doi.org/10.3390/catal13071080

Academic Editors: Tian-Sheng Zhao, Jianli Zhang, Xinhua Gao and Kangzhou Wang

Received: 15 May 2023
Revised: 29 June 2023
Accepted: 6 July 2023
Published: 8 July 2023

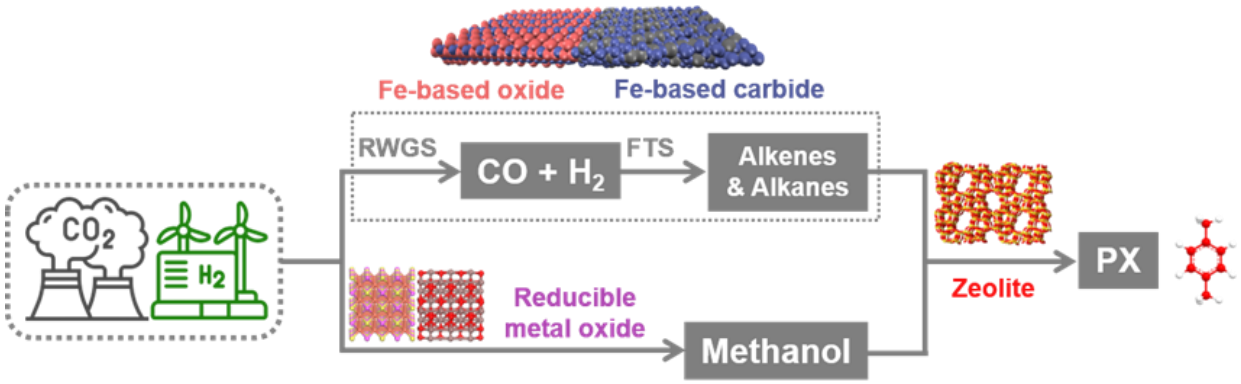
Copyright: © 2023 by the authors. Licensee MDPI, Basel, Switzerland. This article is an open access article distributed under the terms and conditions of the Creative Commons Attribution (CC BY) license (https://creativecommons.org/licenses/by/4.0/).

1. Introduction

As a major contributor to the greenhouse effect, the capture and resource utilization of CO_2 can not only alleviate the trend of global warming but also provide a feasible technical route for the synthesis of high-value-added chemicals [1–3]. CO_2 hydrogenation is currently the most efficient means of CO_2 conversion into valuable chemicals (i.e., methanol, light olefins, aromatics, etc.) due to its high efficiency and industrial applicability [4–6]. Among all of these products, aromatics—especially para-xylene (PX), as the most valuable aromatic hydrocarbons—are basic building blocks in the polymer industries [7]. Compared to the traditional fossil fuel-based PX production pathway, the direct transformation of CO_2 + H_2 into PX holds great potential to alleviate the pressures from the depletion of fossil fuel reserves and environmental issues [8,9]. It is of strategic significance to develop synthetic routes towards aromatic compounds, especially PX, based on the CO_2 hydrogenation process.

Until now, two main pathways have been proposed to realize direct PX synthesis from CO_2 + H_2, including the modified Fischer–Tropsch synthesis (FTS) pathway and the

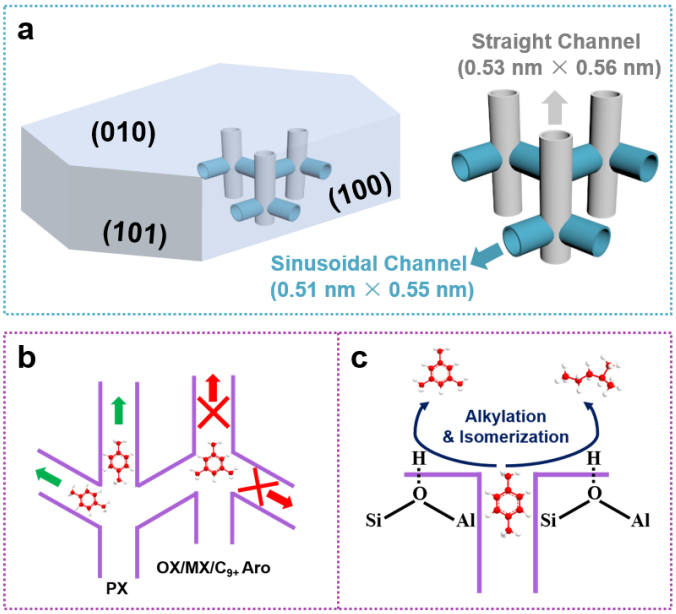
methanol-mediated pathway (Scheme 1) [10,11]. During the modified FTS process, the multifunctional catalyst composed of an Fe-based catalytic component (Fe-based oxide and carbide) and acidic zeolite could cascade the reverse water-gas shift reaction ($CO_2 + H_2 \rightarrow CO + H_2O$), FTS, aromatization process, etc. into a one-pass for PX synthesis [12–16]. For the methanol-mediated pathway, the combination of the methanol synthesis and the classical methanol-to-aromatics (MTA) process via a bifunctional catalyst involved in a reducible metal oxide (e.g., $ZnZrO_x$, $ZnAlO_x$, $ZnCrO_x$, etc.) and acidic zeolite guarantees the direct conversion of $CO_2 + H_2$ into PX [17–22]. It is obvious that no matter which route is chosen, the physicochemical property of the acidic zeolite plays a vital role in altering the selectivity of aromatics, especially the most valuable PX.



Scheme 1. The modified FTS and the methanol-mediated pathways for PX synthesis from CO_2 hydrogenation.

ZSM-5 zeolite with an MFI topology and a three-dimensional 10-membered ring channel system features two distinct types of channels (Scheme 2a): the two-dimensional sinusoidal channel (0.51 nm × 0.55 nm) opening on 100 plane and the straight channel (0.53 nm × 0.56 nm) opening on 010 plane [23,24]. Ideally, the channel structure of ZSM-5 is accommodative for shape-selective PX synthesis due to the close dynamic diameter of PX (ca. 0.58 nm) with the channel structure of ZSM-5. The formation of isomers ortho-xylene (OX) and meta-xylene (MX) as well as the heavy aromatics (C_{9+}) with larger molecular dynamic diameters (>0.68 nm) can be well suppressed by the narrow channels of ZSM-5 (Scheme 2b) [25]. However, the undesirable isomerization and alkylation reactions on the external acid site or at the pore mouth of ZSM-5, without shape-selective function, always lower the PX selectivity in the ZSM-5-catalyzed aromatics synthesis reactions, such as toluene alkylation or MTA (Scheme 2c) [26]. At the same time, owing to the thermodynamic equilibrium limitation and the change in the non-rigid skeleton structure under high reaction temperatures, the molecules with a close dynamic diameter to PX, such as OX and MX, can also diffuse out of the ZSM-5 channels as final products, which is another cause of lowered PX selectivity. For instance, the PX selectivity in X is usually lower than 24% [27]. To tackle above obstacles, much attention has been paid to rationally tailoring the acidic and architectural properties of the ZSM-5. On the one hand, the external acid sites of ZSM-5 can be erased by coating an amorphous SiO_2 layer or epitaxially growing a non-acidic zeolite membrane on the surface of ZSM-5 crystals. This external acid site erasing strategy has been widely employed to boost the PX selectivity of several ZSM-5-catalyzed reactions, such as toluene alkylation, MTA, syngas conversion, and CO_2 hydrogenation [28–32]. However, it should be noted that the adhesion of amorphous SiO_2 and non-acidic zeolite onto the external surface of ZSM-5 will inevitably decrease the reactivity due to the loss of acid site. On the other hand, considering that the shape-selective capability of the sinusoidal channels with smaller pore size, predominantly opening on the 100 crystal plane of ZSM-5, is stronger than that of the straight channels with larger pore size, primarily opening on the 010 crystal plane, the precise control of the priority exposure

of 100 crystal plane, i.e., increasing the opening of sinusoidal channels, has been proven to be feasible in optimizing the PX selectivity by tailoring the diffusion behaviors of PX and the isomers in the elongated channels. Recently, Ma et al. synthesized a twin-structured ZSM-5 for toluene alkylation with methanol, in which the intergrowth morphology with 100-plane-dominated twin crystal covering the body crystal maximizes the exposure of sinusoidal channels, therefore optimizing the shape-selective capability of ZSM-5 for PX synthesis (>99% PX selectivity) [33]. Furthermore, this twin-structured ZSM-5 possessed a decreasing acid site density gradient from the core to the surface. The surface with poor acidic sites could prohibit the undesirable side reactions that occurred on the external surface or in the pore mouth of ZSM-5 due to the decreased accessibility of reactive centers, which is another key factor in boosting PX selectivity. Tsubaki et al. explored the possibility of this twin-structured ZSM-5 in tandem catalysis of CO_2 + H_2 into PX via the methanol-mediated pathway. Interestingly, after combining this twin-structured ZSM-5 zeolite with $ZnCr_2O_4$, which can convert CO_2 into methanol efficiently, high PX/X and PX/aromatics ratios of 97.3% and 63.9% were achieved, respectively [34]. Sun et al. presented a series of novel HZSM-5 nanocrystal clusters with chain-like morphology and chain length. With the combination of highly active $ZnZrO_x$ oxides, the composite catalyst achieved excellent performance of CO_2 hydrogenation to aromatics. They found that a proper extension of the b-axis length and passivation of external surface acid sites of HZSM-5 could greatly enhance the selectivity of PX [35]. Tsubaki et al. tailored the physicochemical properties of the parent H-ZSM-5 by metal ion doping and subsequent SiO_2 coating to study the effect of the zeolite component on the aromatics synthesis performance from syngas. The strong CO adsorption capacity and the lower C-C coupling barrier derived from Ga doping guaranteed the superior aromatics yield. The blocking of the external acid sites of H-ZSM-5 by SiO_2 deposition is beneficial to suppress the undesirable side reactions, therefore boosting light aromatics synthesis [36]. Even though great progress has been made in the rational design of the ZSM-5 zeolitic component to enhance the PX selectivity of various ZSM-5-catalyzed aromatics synthesis reactions, there is still a lack of innovative works on optimizing PX synthesis performance by systematically considering most of the essential factors that affect the shape-selective property of ZSM-5.



Scheme 2. (**a**) The topology structure of ZSM-5 (the gray arrow represents the straight channel, and the blue arrow represents the sinusoidal channel), (**b**) shape-selective synthesis of ZSM-5 (the green arrows mean that the products could pass the channels easily, while the red arrows mean it is difficult to pass), and (**c**) side reactions that occurred on the external surface or at the pore mouth of ZSM-5.

In this work, we focus on enhancing the PX selectivity of the methanol-mediated tandem CO_2 hydrogenation process by simultaneously tailoring the architectural and acidic properties of the ZSM-5 component in the bifunctional catalyst. The twin-structured ZSM-5 zeolite is employed as an initial research subject. To further increase its shape-selective capability, an amorphous SiO_2 shell is coated onto the external surface to erase the undesirable acid sites. More importantly, to eliminate the negative effect brought about by SiO_2 deposition, i.e., the loss of catalytic reactivity stemming from the decrease in the amount of acid sites, Cu ions, which are widely used to enrich the acid site density and tailor the acidic property of zeolite, are exchanged into the zeolite framework to strengthen the driving force in the tandem process. Benefiting from this comprehensive regulation strategy, the PX selectivity from CO_2 hydrogenation could clearly be improved. We hope that our work will provide new insights into the rational design of ZSM-5 zeolite with excellent shape-selective ability.

2. Results

2.1. Physicochemical Property of the Twin-Structured Zeolite

The twin-structured ZSM-5 zeolite (denoted as H-ZSM-5^T) was prepared by the traditional hydrothermal method. Cu ions were exchanged into the zeolite framework to enrich the acid site density and tailor the acidic property of H-ZSM-5^T. It should be noted that in our previous work, the transition metals, such as Zn, Ga, La, Mg, etc., were doped into the zeolitic framework to investigate their effects on tailoring the catalytic performance of H-ZSM-5 zeolite in the methanol-mediated conversion of CO_2 + H_2 or syngas into aromatics. However, the effect of Cu ions has been rarely clarified. Finally, a non-acidic and amorphous SiO_2 shell was coated onto the external surface of Cu-ZSM-5^T to further suppress the undesirable alkylation and isomerization reactions that usually occurred on the external surface. The final catalyst was denoted as Cu-ZSM-5^T@SiO_2.

Multiple techniques were employed to examine the physicochemical properties of the obtained zeolitic catalysts. The X-ray fluorescence (XRF) spectra verified that the Si/Al ratio in H-ZSM-5^T is ca. 70. The X-ray diffraction (XRD) patterns of H-ZSM-5^T, Cu-ZSM-5^T, and Cu-ZSM-5^T@SiO_2 are depicted in Figure 1. All of these three zeolites exhibited typical characteristics of MFI zeolite structure, with notable peaks at 7°, 8°, 23°, and 24°, which were attributed to the (101), (200), (332), and (303) crystal planes of MFI-type zeolite (PDF#44-0003), confirming the successful synthesis of H-ZSM-5 zeolite. The following Cu ion exchange and SiO_2 coating steps had no influence on the crystal structure of the samples. No diffraction peaks of Cu species were detected in the XRD patterns, confirming that the ion exchange strategy guarantees the homogeneous dispersion of them in the zeolitic framework.

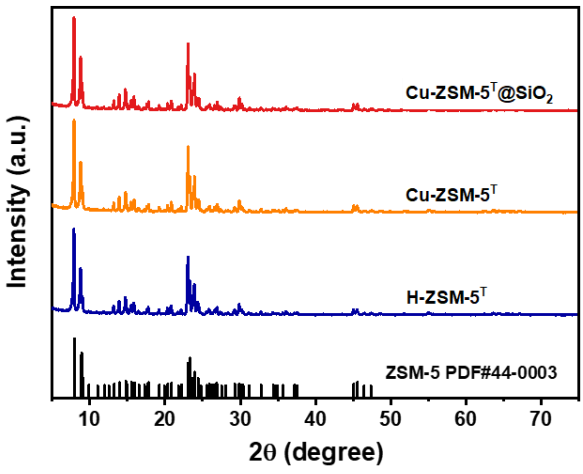


Figure 1. XRD patterns of H-ZSM-5^T, Cu-ZSM-5^T, and Cu-ZSM-5^T@SiO_2.

Scanning electron microscopy (SEM) images (Figure 2a) revealed that the synthesized H-ZSM-5^T had a grain size of approximately 8 μm along the c-axis, a relatively smooth surface, and an obvious intergrowth structure. Specially, in the case of a single crystal, the body crystal was mostly covered by an intergrowth twin crystal (Figure 2b). The texture property of this twin-structured zeolite has been clarified in detail by Ma et al. On the basis of their high-resolution microscopy, selected-area electron diffraction (SAED), and laser confocal fluorescence results, it is clearly demonstrated that the two 010 planes (up and down) of each main crystal with straight channel openings was mostly covered by two independent twin crystals, and the 100 planes with sinusoidal channel openings were well maintained (Figure 2c and Scheme 2). Owing to the fact that the two independent twin crystals mainly exposed the 100 planes with sinusoidal channels opening along the a-axis, the final twin-structured H-ZSM-5^T maximized the opening of sinusoidal channels, accounting for 73% of the total openings on the external surface, which is a great deal higher than that of the classical coffin-shape H-ZSM-5 (ca. 43%). This unique characteristic of sinusoidal channel maximization exposure will enhance the shape-selective capability of the H-ZSM-5 zeolite. The morphology of Cu-ZSM-5^T obtained by ion exchange treatment was nearly identical to that of H-ZSM-5^T (Figure 2d). However, the SiO_2-coated Cu-ZSM-5^T@SiO_2 catalyst was significantly different from the other two samples, as evidenced by the aggregation between zeolitic crystals (Figure 2e,f). The amorphous SiO_2 shell enwrapped several Cu-ZSM-5^T crystals to fabricate the core-shell structured capsule catalyst, in which the undesirable external acid sites could be eliminated to some extent. The SEM energy dispersive spectroscopy (EDS) mapping images, as shown in Figure 3, indicated that the Si, Al, and Cu elements are uniformly distributed throughout the synthesized Cu-ZSM-5^T@SiO_2 capsule catalyst. In particular, the strong Si signals confirmed the successful and complete encapsulation of the twin-structured zeolites by the non-acidic SiO_2 shell. Moreover, no regional enrichment of Cu species was detected in the EDS mapping images due to the homogeneous distribution in the zeolite framework, which is in line with the XRD results. Only 1.7 wt% Cu was doped into Cu-ZSM-5^T as characterized by XRF, and this value could decrease after SiO_2 deposition. As we know, Cu nanoparticles are ideal catalytic components of hydrogenation reaction. During the MTA process catalyzed by acidic zeolite, the existence of Cu nanoparticles could facilitate the hydrogenation of the key reaction intermediates (e.g., unsaturated alkenes or cyclo-alkenes), which is contrary to the dehydrogenation reaction mechanism for aromatics synthesis. Herein, the homogeneously dispersed Cu species (even single atoms) in Cu-ZSM-5^T@SiO_2 will mainly play their roles in tailoring the acidic property of the zeolite rather than delivering the hydrogenation functions due to the low Cu content and even dispersion in zeolite skeleton. One may also wonder whether the Cu species in acidic zeolite catalyze CO_2 + H_2 into methanol because Cu-based catalysts are ideal components for methanol synthesis from syngas or CO_2 + H_2. However, the low Cu content and the homogeneous dispersion in the zeolite skeleton, as confirmed by the XRD, XRF, and SEM-EDS results, make them difficult to use for methanol synthesis. We tested the CO_2 hydrogenation performance of the sole Cu-ZSM-5^T catalytic component under 350 °C and 3 MPa, and Cu-ZSM-5^T exhibited no CO_2 hydrogenation activity, which again verifies our viewpoint.

N_2 adsorption and desorption tests were performed on the aforementioned three catalysts to investigate the impacts of Cu doping and SiO_2 coating on the specific surface area and pore structure of the zeolites. As demonstrated in Figure 4a, H-ZSM-5^T, Cu-ZSM-5^T, and Cu-ZSM-5^T@SiO_2 all displayed type-I(b) N_2 adsorption and desorption isotherms. The rapid N_2 absorption at low relative pressures indicated that these three zeolitic components consist primarily of micropores. The hysteresis loop at P/Po ~ 0.1 can be ascribed to pore filling into supermicropores or small mesopores [37]. The pore size distribution obtained using the DFT model provided additional evidence of the microporous property of the zeolites (Figure 4b). Additionally, as indicated in Table 1, the specific surface area of H-ZSM-5^T, Cu-ZSM-5^T, and Cu-ZSM-5^T@SiO_2 declined gradually. This suggests that the introduction of Cu ions occupied part of the pore of the parent H-ZSM-5^T

zeolite, leading to a decrease in the specific surface area of the Cu-ZSM-5^{T} from 376 m^2 g^{-1} to 372 m^2 g^{-1}. Furthermore, subsequent deposition of SiO_2 shell on the exterior of the zeolite obstructed the pore mouth of the microporous surface, resulting in further reduction in the specific surface area of Cu-ZSM-5^{T}@SiO_2 to 363 m^2 g^{-1}. The BET surface area of the three zeolites was indeed very similar, but the microporous and mesoporous specific surface area exhibited a clear variation pattern. Compared to H-ZSM-5^{T}, the microporous specific surface area of Cu-ZSM-5^{T} decreased from 144 m^2 g^{-1} to 129 m^2 g^{-1}, indicating that Cu ions occupied part of the micropores of the parent H-ZSM-5^{T} zeolite. Furthermore, subsequent deposition of SiO_2 shell on the exterior of the zeolite obstructed the pore mouth of the microporous surface, and the microporous-specific surface area of Cu-ZSM-@SiO_2 reduced to 78 m^2 g^{-1}. The increase in mesoporous-specific surface area of Cu-ZSM-@SiO_2 was attributed to the mesoporous property of SiO_2.

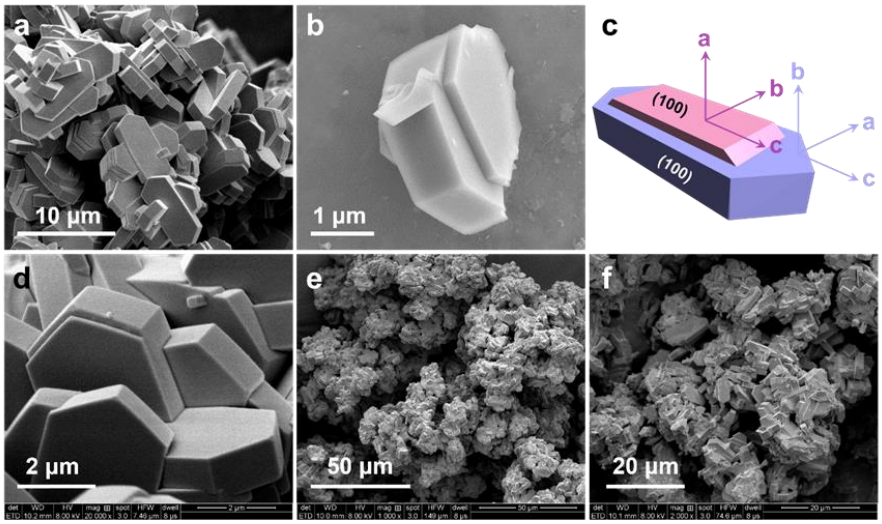


Figure 2. (**a**,**b**) SEM images of H-ZSM-5^{T}, (**c**) I schematic illustration of the twin-structured zeolite (The a-axis, b-axis, and c-axis are perpendicular to the 100, 010, and 101 crystal planes, respectively), SEM image of Cu-ZSM-5^{T}, (**d**) and Cu-ZSM-5^{T}@SiO_2 (**e**,**f**).

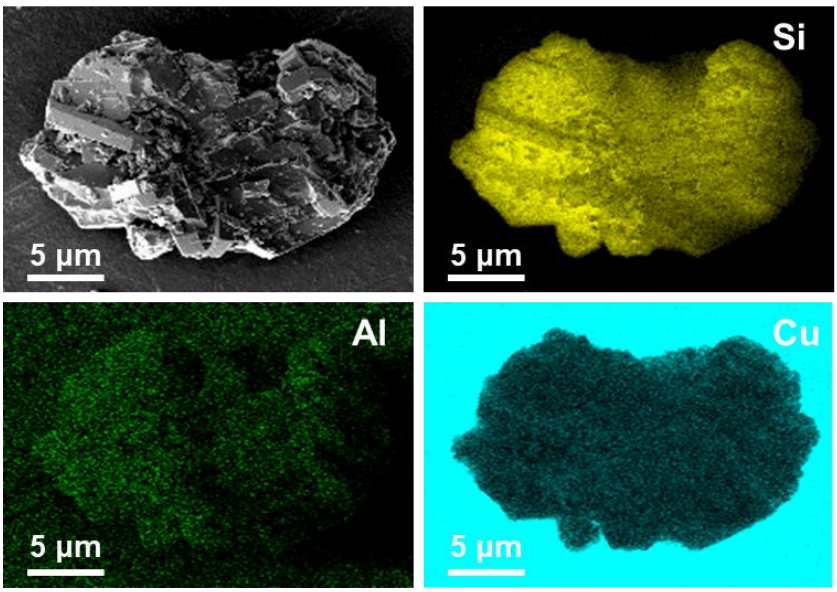


Figure 3. SEM EDS mapping images of Si, Al, and Cu elements in the Cu-ZSM-5^{T}@SiO_2 capsule catalyst.

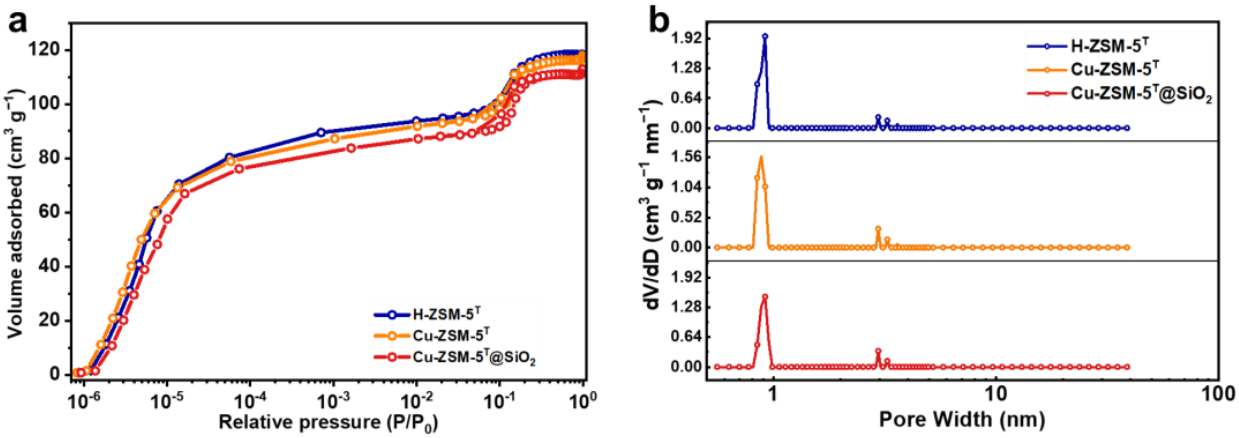


Figure 4. (**a**) Nitrogen adsorption-desorption isotherms of H-ZSM-5^T, Cu-ZSM-5^T, and Cu-ZSM-5^T@SiO$_2$, and (**b**) pore size distribution calculated by DFT model.

Table 1. Texture property of H-ZSM-5^T, Cu-ZSM-5^T, and Cu-ZSM-5^T@SiO$_2$.

Catalyst	S_{BET} (m^2/g)	S_{micro} (m^2/g)	S_{meso} (m^2/g)	Average Pore Diameter (nm)
H-ZSM-5^T	376	144	232	1.95
Cu-ZSM-5^T	372	129	242	1.96
Cu-ZSM-5^T@SiO$_2$	363	78	285	1.92

The acid properties of H-ZSM-5^T, Cu-ZSM-5^T, and Cu-ZSM-5^T@SiO$_2$ were evaluated using NH_3 temperature-programmed desorption experiments. As shown in Figure 5, two distinctive NH_3 desorption peaks appeared in all three catalysts, including the low-temperature peak that corresponded to the weak acid sites and the high-temperature peak that corresponded to the medium/strong acid sites. Compared to H-ZSM-5^T, the NH_3 desorption peak of Cu-ZSM-5^T shifted to higher temperatures, indicating the enhanced acid strength due to the formation of Lewis acid sites after Cu ion doping and the synergistic effect between the Brønsted and Lewis acid sites. Meanwhile, the NH_3 desorption peak of Cu-ZSM-5^T@SiO$_2$ slightly shifted to the low-temperature region relative to Cu-ZSM-5^T due to SiO_2 deposition on the external surface of the zeolite, leading to the shielding of some acidic sites and the slight weakening of the adsorption capacity for NH_3 molecules. The reduction in the undesirable acid sites can suppress undesirable isomerization and alkylation reactions, thereby boosting the PX selectivity [35]. Nonetheless, the acid strength of Cu-ZSM-5^T@SiO$_2$ remained greater than that of H-ZSM-5^T. Benefiting from the enhanced acid strength after Cu ion doping, the consumption of the reaction intermediates by acid zeolites could be facilitated, therefore continuously and efficiently cleaning up the catalytic interface for intermediate synthesis and shifting the tandem process forward [36].

To analyze the strength of the basic sites of H-ZSM-5^T, Cu-ZSM-5^T, and Cu-ZSM-5^T@SiO$_2$, the CO_2-TPD experiments were conducted. As Figure 6 shows, all three zeolites displayed one desorption peak in the range of 100~200 °C, which implied that they contained predominantly weak basic sites. As we know, the Brønsted (Si-OH-Al) and Lewis acid (derived from Cu species) in zeolite are the key active sites for methanol conversion into aromatics via dehydration, dehydrogenation, and aromatization steps, and the basic site is deemed to be harmful for aromatics synthesis.

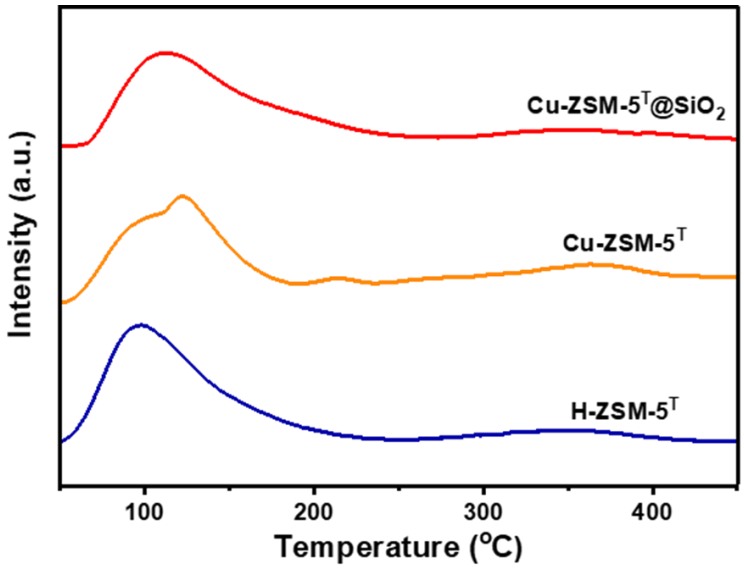


Figure 5. NH_3-TPD profiles of H-ZSM-5^T, Cu-ZSM-5^T, and Cu-ZSM-5^T@SiO_2.

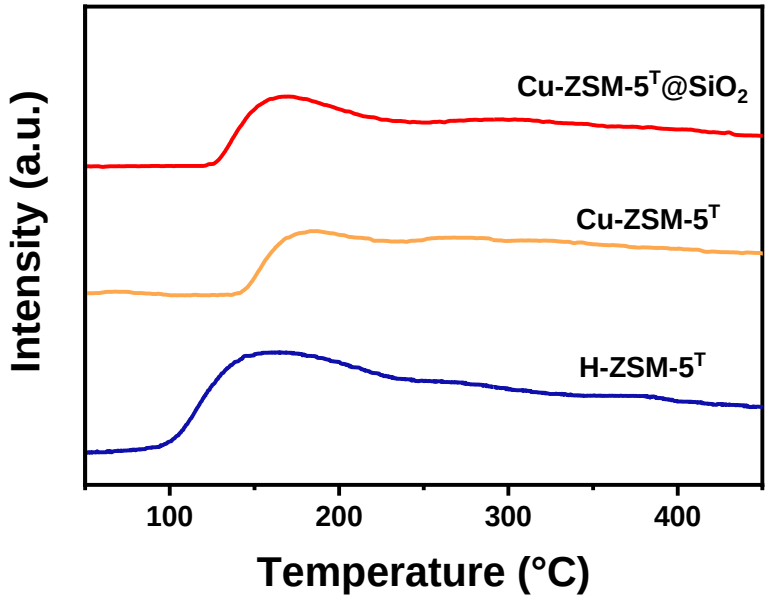


Figure 6. CO_2-TPD profiles of H-ZSM-5^T, Cu-ZSM-5^T, and Cu-ZSM-5^T@SiO_2.

The Cr_2O_3-based catalyst was prepared by subsequently carbonizing and oxidizing the Cr-based metal-organic frameworks' (MOFs') precursors (denoted as Cr_2O_3/C). The MOFs-derived Cr_2O_3/C catalyst exhibited excellent methanol selectivity of 98.1% (without CO) at a CO_2 conversion of 16.8%. The detailed physicochemical properties of the Cr_2O_3/C catalyst have been investigated in our previous work with the aid of multiple characterization techniques [38]. In this work, we mainly paid attention to improving the PX synthesis performance of the acidic zeolite. The bifunctional catalyst was prepared by physically grinding the methanol synthesis Cr_2O_3/C catalyst and the acidic zeolite component. With Cr_2O_3/C&Cu-ZSM-5^T as an example, the nanoscale morphology of the bifunctional catalyst was observed by SEM. As shown in Figure 7, the Cr_2O_3/C nanoparticles with loose and spherical morphology distributed on the external surface of Cu-ZSM-5^T homogeneously. The nanoscale size of Cr_2O_3/C is favorable to enhance the proximity between different catalytic components by increasing the contact area. It should be noted that for tandem catalysis of CO_2 + H_2 into aromatics, the close proximity between different catalytic components is essential. On the one hand, the close proximity is beneficial for

transporting the reaction intermediates from reducible metal oxide to the acidic zeolite for aromatics synthesis via the tandem process. On the other hand, the aromatics synthesis process follows the dehydrogenation mechanism. The continuous extraction of H* species from the zeolite component is the prerequisite for the success of aromatics synthesis. The reducible metal oxide as the H* species acceptor and consumer plays a key role during the dehydrogenation process by extracting and consuming the H* species, and the close proximity between the reducible metal oxide and acidic zeolite could facilitate this dehydrogenation process, therefore boosting the aromatics synthesis process.

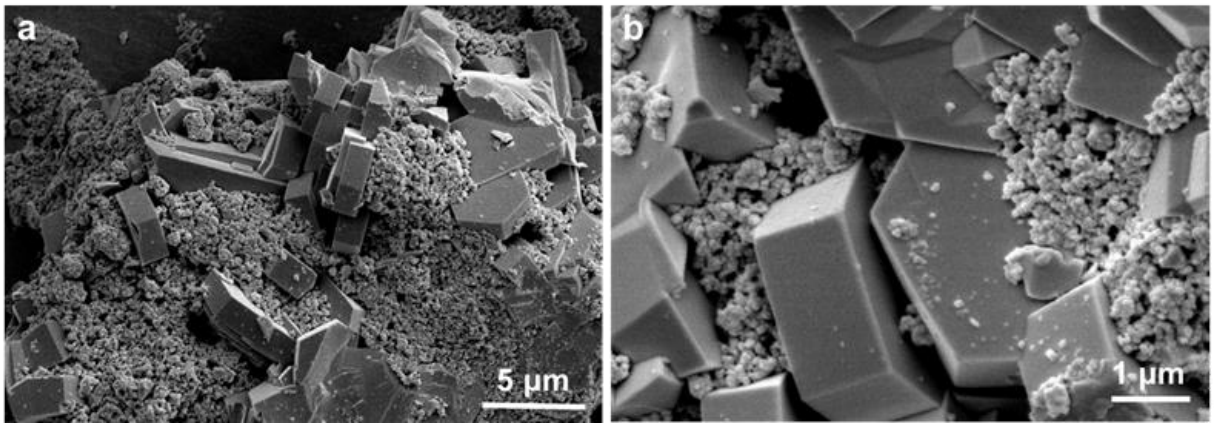


Figure 7. (**a**,**b**) SEM images of Cr_2O_3&H-ZSM-5^T.

2.2. The Catalytic Performance of PX Synthesis from CO_2 Hydrogenation

To investigate the effect of different catalysts on PX selectivity, a CO_2 hydrogenation reaction of Cr_2O_3/C&H-ZSM-5^T, Cr_2O_3/C&Cu-ZSM-5^T, and Cr_2O_3/C&Cu-ZSM-5^T@SiO_2 was conducted under 350 °C and 3 Mpa (Figure 8, Tables 2 and 3). Cr_2O_3/C&H-ZSM-5^T exhibited an aromatics selectivity of 78.7% at a CO_2 conversion of 17.2%, with PX selectivity reaching 28.7%. The PX selectivity obtained from the bare H-ZSM-5^T zeolite significantly outperformed that of the classical coffin-shape H-ZSM-5, which can be attributed to the unique twin structure with dominant sinusoidal channel openings. After Cu ion doping and CO_2 conversion, the aromatics selectivity of Cr_2O_3/C&Cu-ZSM-5^T increased to 19.2% and 80.4%, respectively, while the PX selectivity decreased slightly (27.4%). This catalytic performance variation trend confirmed that Cu ion doping is favorable to increase the CO_2 transformation efficiency and the total aromatics selectivity due to the enhanced acid strength and aromatization capability of Cu-ZSM-5^T. Even though Cu ion doping slightly increased the space-time yield (STY) of PX, owing to the enhanced CO_2 conversion, the PX selectivity from Cr_2O_3/C&Cu-ZSM-5^T was decreased due to the reduced shape-selective capability of Cu-ZSM-5^T. There is no doubt that the Cu ions in the zeolite framework could act as Lewis acid sites, as well as enhance the acid strength by cooperating with the originally existing Brønsted acid, but the ion exchange strategy could also introduce undesirable acid sites on the external surface or pore mouth of microporous channels of Cu-ZSM-5^T, therefore decreasing its shape-selective property.

Therefore, our attention turned to erasing the undesirable external acid sites by coating a non-acidic SiO_2 shell onto the external surface of Cu-ZSM-5^T by chemical liquid deposition. Benefiting from the cooperative interplay between the enhanced acid strength via Cu ion doping and the erasing of the undesirable acid sites via SiO_2 shell coating, the selectivity of total aromatics and PX were increased to 82.3% and 33.8%, respectively, via the bifunctional catalyst of Cr_2O_3/C&Cu-ZSM-5^T@SiO_2. Even though the CO_2 conversion slightly decreased to 18.4%, the STY of PX from Cr_2O_3/C&Cu-ZSM-5^T@SiO_2 (3.0 g_{CH2} h^{-1} $kg_{cat}{}^{-1}$) was superior to that from the counterparts Cr_2O_3/C&H-ZSM-5^T (2.5 g_{CH2} h^{-1} $kg_{cat}{}^{-1}$) and Cr_2O_3/C&Cu-ZSM-5^T (2.6 g_{CH2} h^{-1} $kg_{cat}{}^{-1}$).

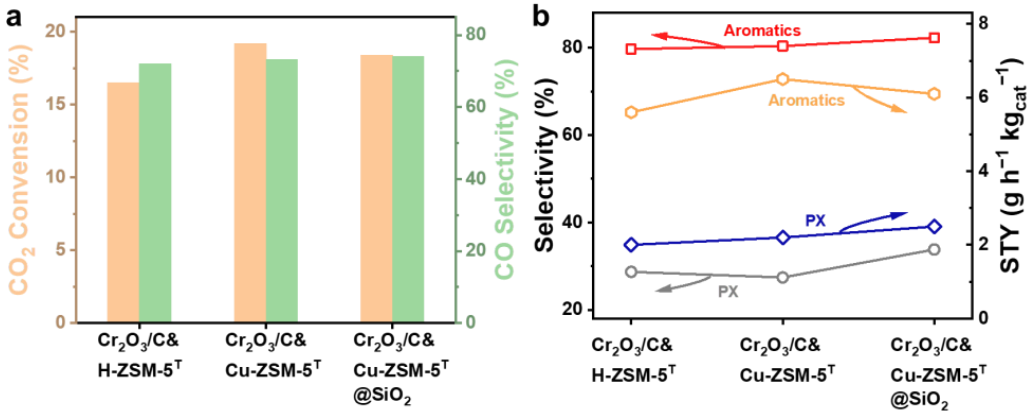


Figure 8. Catalytic performance of the bifunctional catalysts composed of Cr_2O_3/C and H-ZSM-5^T or Cu-ZSM-5^T or Cu-ZSM-5^T@SiO_2: (**a**) CO_2 conversion and CO selectivity, (**b**) space-time yield of (STY) and selectivity of PX and aromatics. Reaction conditions: 350 °C, 3 Mpa, (24.3% CO_2, 71.8% H_2, and 3.9% Ar), GHSV = 1200 mL g_{cat}^{-1} h^{-1}, time on stream (TOS) = 8 h, metal oxide/zeolite mass ratio = 1, and catalyst of 1 g.

Table 2. Catalytic performance of Cr_2O_3/C&H-ZSM-5^T, Cr_2O_3/C&Cu-ZSM-5^T, and Cr_2O_3/C&Cu-ZSM-5^T@SiO_2 for CO_2 hydrogenation into aromatics [a].

Catalysts	CO_2 Conv. (%)	CO Sel. (%)	Hydrocarbon Distribution (%)				
			CH_4	C_2^0-C_4^0	$C_2^=$-$C_4^=$	CH_3OH	Aromatics
Cr_2O_3/C&H-ZSM-5^T	16.5	72.1	2.3	9.5	9.1	0.4	78.7
Cr_2O_3/C&Cu-ZSM-5^T	19.2	73.2	3.6	8.5	7.2	0.3	80.4
Cr_2O_3/C&Cu-ZSM-5^T@SiO_2	18.4	74.1	1.7	9.1	6.6	0.3	82.3

[a] Reaction conditions: 350 °C, 3 Mpa, (24.3% CO_2, 71.8% H_2, and 3.9% Ar), GHSV = 1200 mL g_{cat}^{-1} h^{-1}, time on stream (TOS) = 8 h, metal oxide/zeolite mass ratio = 1, and catalyst of 1 g.

Table 3. Products distribution in aromatics.

Catalysts	Selectivity of Aromatics (%) [a]							STY of PX (g_{CH2} h^{-1} kg_{cat}^{-1})
	B	T	E	PX	OX	MX	A(C_{9+})	
Cr_2O_3/C&H-ZSM-5^T	0.5	5.0	1.4	28.7	6.3	1.3	35.5	2.5
Cr_2O_3/C&Cu-ZSM-5^T	0.7	4.5	0.4	27.4	6.8	1.5	39.1	2.6
Cr_2O_3/C&Cu-ZSM-5^T@SiO_2	0.9	6.6	1.8	33.8	7.5	1.2	30.5	3.0

[a] The selectivity of B, T, E, PX, OX, and A (C_{9+}) in all of the products, in which B = Benzene, T = Toluene, E = ethylbenzene, PX = para-xylene, MX = meta-xylene, and OX = ortho-xylene.

3. Materials and Methods

3.1. Materials and Chemicals

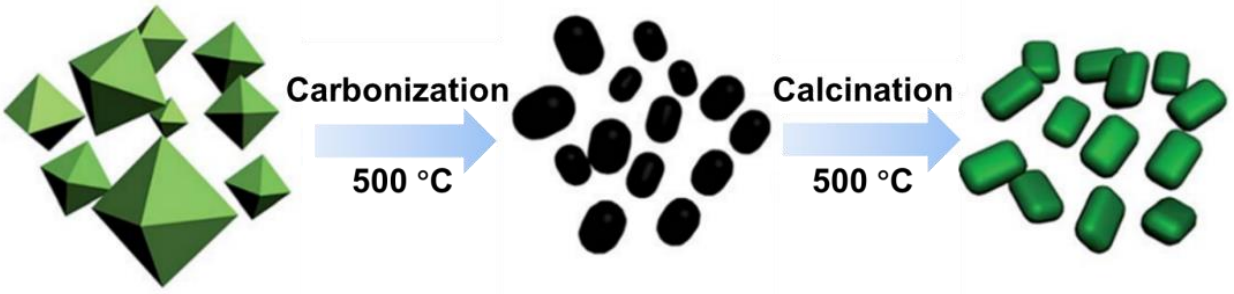
The chromium nitrate nonahydrate [$Cr(NO_3)_3 \cdot 9H_2O$], terephthalic acid (PTA), concentrated nitric acid, sodium aluminate ($NaAlO_2$), tetrapropylammonium bromide (TPABr), n-butylamine, silica sol, copper nitrate trihydrate [$Cu(NO_3)_2 \cdot 3H_2O$], ethanol, n-hexane, and tetraethyl orthosilicate (TEOS) that purchased from Aladdin Biochemical Technology Co., Ltd (Shanghai, China) were of analytical grade and utilized without further purification. The deionized water used for catalyst preparation had a resistivity of 18.2 megohms and was obtained through an ultrapure water system (Milli-Q, Merck, Germany).

3.2. Catalyst Preparation

3.2.1. Synthesis of Cr_2O_3/C Catalyst

Scheme 3 shows the preparation process of MOFs-derived, Cr-based catalysts. Cr-MOFs were synthesized via a hydrothermal method. Typically, $Cr(NO_3)_3 \cdot 9H_2O$ of

10.0 mmol (4.00 g) and PTA of 10.0 mmol (1.66 g) were dissolved into the deionized water of 48 mL. Subsequently, concentrated nitric acid of 680 µL was added dropwise under stirring, and the mixture was stirred for 30 min to ensure complete phase dispersion. The resulting solution was transferred into an 80 mL Teflon-lined autoclave and kept at 220 °C for 8 h. Green crystalline products obtained after centrifugation underwent washing three times with deionized water and ethanol, followed by drying overnight at 60 °C in an oven. These products were then pyrolyzed at 500 °C for 2 h in a tube furnace under an N_2 atmosphere with a heating rate of 5 °C min^{-1} to obtain the black powders. Finally, calcination of the aforementioned powders was undertaken at 500 °C for 2 h in a muffle furnace under air atmosphere with a heating rate of 5 °C min^{-1} yielded the Cr-based catalyst, denoted as Cr_2O_3/C.



Scheme 3. Preparation process of MOFs-derived Cr-based catalysts.

3.2.2. Synthesis of H-ZSM-5^T

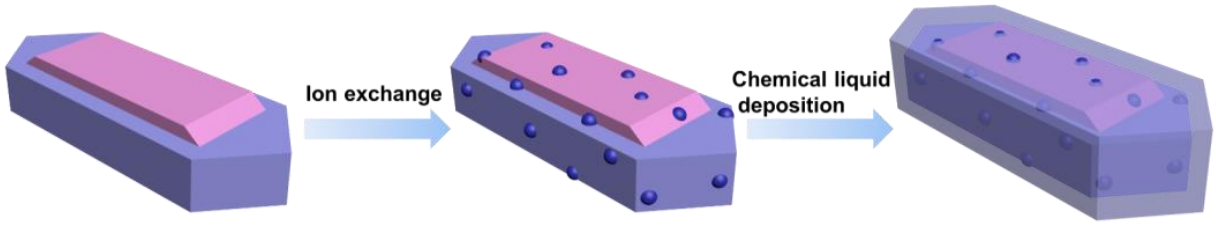
An H-ZSM-5^T zeolite with twin-structure was synthesized via a hydrothermal method. $NaAlO_2$ (0.080 g), TPABr (1.834 g), and n-butylamine (3.916 g) were dissolved into 91.5 mL of deionized water by stirring for 15 min. Subsequently, silica sol of 22.53 g was slowly added dropwise under stirring for 30 min. The resulting solution was divided evenly into two 80 mL Teflon-lined autoclaves, fixed on the rotary support of a rotary blast drying oven, and kept at a temperature of 180 °C for 48 h with rotating speed of 1.5 rpm. The obtained emulsion was centrifugally washed three times by deionized water, followed by drying overnight at 60 °C to acquire the H-ZSM-5^T precursor. Calcination of the precursor was undertaken at 550 °C for 6 h in a muffle furnace with a heating rate of 5 °C min^{-1} to remove the organic template in H-ZSM-5^T.

3.2.3. Synthesis of Cu-ZSM-5^T

The Cu-H-ZSM-5^T zeolite was synthesized via an ion exchange method. Initially, $Cu(NO_3)_2 \cdot 3H_2O$ (6.5 mmol, 1.57 g) was dissolved into 91.5 mL of deionized water, followed by the addition of H-ZSM-5^T of 1.3 g under stirring. The resulting mixture was moved to an 80 °C oil bath and stirred for 15 h for ion exchange. After ion exchange, the product was centrifugally washed three times by deionized water and dried overnight at 60 °C in an oven. The dried product was then calcined at 500 °C for 3 h in a muffle furnace to yield the Cu-ZSM-5^T zeolite.

3.2.4. Synthesis of Cu-ZSM-5^T@SiO_2

The Cu-ZSM-5^T@SiO_2 capsule catalyst was obtained by employing TEOS to coat the external surface of Cu-ZSM-5^T via a chemical liquid deposition method. Initially, Cu-ZSM-5^T of 1 g was dispersed into n-hexane of 8 mL via ultrasonication for 15 min to prevent agglomeration. Next, TEOS of 2.25 g was slowly added dropwise to the solution under stirring for 4 h. The resulting mixture was further transferred to an 80 °C oil bath until complete evaporation of n-hexane. Finally, the coated molecular sieve was calcined at 500 °C for 2 h in a muffle furnace with a heating rate of 5 °C min^{-1} to yield the Cu-ZSM-5^T@SiO_2 capsule catalyst. Scheme 4 shows the preparation process of Cu-ZSM-5^T and Cu-ZSM-5^T@SiO_2.



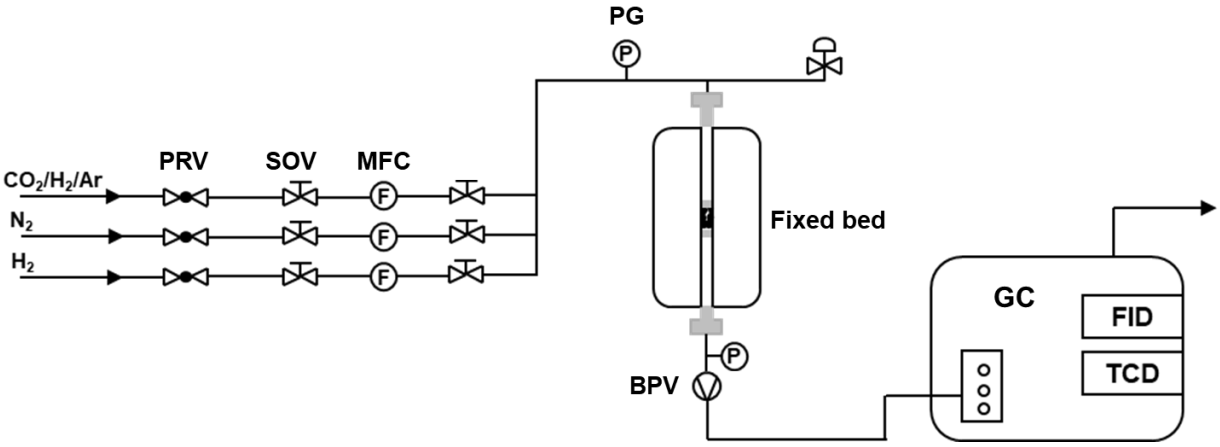
Scheme 4. Preparation process of Cu-ZSM-5^{T} and Cu-ZSM-5^{T}@SiO_2.

3.3. Catalyst Characterization

X-ray diffraction (XRD) analysis of the obtained catalysts was conducted using Cu Kα radiation and a Rigaku RINT 2400 X-ray diffractometer (Tokyo, Japan). The morphology of the catalysts was observed via scanning electron microscopy (SEM) on a Zeiss Genimi 300 instrument (Oberkochen, Germany) equipped with an energy dispersive spectroscopy (EDS) system using an Oxford Inca Energy X-max 50 X-ray EDS detector. Furthermore, the specific surface area and pore size distribution of the samples were determined by a Micromeritics 3Flex 2MP instrument (Norcross, GA, USA). The surface area was determined by the Brunauer–Emmett–Teller (BET) method using a relative pressure (P/P_o) in the range of 0.05–0.3. The pore size distribution was calculated by the non-local density functional theory (NLDFT) method. NH_3 temperature-programmed desorption (NH_3-TPD) and CO_2 temperature-programmed desorption (CO_2-TPD) experiments were carried out on a MicrotracBEL BELCATII-T-SP instrument (Osaka, Japan). Prior to the experiment, the catalyst was pretreated at 150 °C for 1 h to eliminate the H_2O present in the microporous zeolite. Subsequently, the sample was saturated with NH_3 or CO_2 at 50 °C and the physisorbed NH_3 or CO_2 was removed using a He flow. Furthermore, the desorption of NH_3 or CO_2 was recorded under an He flow with a heating rate of 10 °C min^{-1}. X-ray fluorescence (XRF) spectroscopy was employed to evaluate the Si/Al ratio in H-ZSM-5^{T} and the Cu content in Cu-ZSM-5^{T}.

3.4. Catalytic Activity Evaluation

Scheme 5 shows the CO_2 hydrogenation reactor for investigating the activities of the catalysts. The catalytic performance of the catalysts was measured in a fixed-bed reactor (ZXBLUE Co., Ltd., Beijing, China) with an internal diameter of 8 mm. Prior to the reaction, the catalyst was reduced by pure H_2 at 400 °C for 2 h. After cooling down to the room temperature, the reactant gas (24.3% CO_2, 71.8% H_2, and 3.9% Ar) was fed into the reactor until the pressure reached 3 MPa. At the same time, the temperature of the reactor was increased to 350 °C. The exhaust gas was analyzed by an online gas chromatograph (Fuli 9790II, Fuli Analytical Instruments Co., Ltd., Zhejiang, China) equipped with two detectors (thermal conductivity detector (TCD) and flame ionization detector (FID)). The TCD was connected to the TDX-01 (60–80 mesh, 3 mm × 2 m) and Porapak-Q (60–80 mesh, 3 mm × 1 m) packed columns for the analysis of Ar, CO, CH_4, and CO_2, and the FID was connected to the HP-PLOT/Q capillary column (0.53 mm × 30 m) to detect gas-phase hydrocarbons. An off-line gas chromatograph (Fuli 9790II, Fuli Analytical Instruments Co., Ltd., Zhejiang, China) equipped with an FID and two separated columns (DB-1 and DB-WAX) was employed to further identify the xylene isomers in the collected liquid products. In order to suppress the possible condensation during the reaction process, the pipeline from the catalyst bed to the gas chromatograph was heated at 190 °C. This type of catalytic performance test instrument is highly efficient due to the advantage of quick and in-time product analysis.



Scheme 5. Schematic of CO_2 hydrogenation reactor.

CO_2 conversion and product selectivity were calculated by the following equations.

(1) CO_2 conversion was calculated according to:

$$CO_2\ Conversion = \frac{CO_{2\ inlet} - CO_{2\ outlet}}{CO_{2\ inlet}} \times 100\%$$

where $CO_{2\ inlet}$ and $CO_{2\ outlet}$ represent moles of the CO_2 at the inlet and outlet, respectively.

(2) Product selectivity was calculated as the percentage of CO_2 converted into a given product and according to:

$$Sel_i = \frac{N_i \times n_i}{\sum_1^i (N_i \times n_i)} \times 100\%$$

where N_i and n_i represent the mole percentage and carbon number of product *i*.

(3) CO selectivity was calculated according to:

$$CO\ selectivity = \frac{CO_{outlet}}{CO_{2\ inlet} - CO_{2\ outlet}} \times 100\%$$

Typically, the experimental data after the reaction of 8 h were used for discussion.

4. Conclusions

In conclusion, an efficient bifunctional catalyst composed of an MOFs-derived Cr_2O_3/C and Cu ion doped H-ZSM-5^T capsule catalyst has been developed for the direct conversion of CO_2 + H_2 into valuable aromatics, especially PX, via the methanol-mediated tandem process. We proposed a comprehensive strategy to boost the PX selectivity, in which the texture and acid properties of the acidic zeolite were systematically considered. The twin-structured H-ZSM-5^T with dominant sinusoidal channel openings was beneficial for increasing the PX selectivity owing to its enhanced shape-selective capability and controlled PX diffusion dynamic. Furthermore, Cu ion doping and SiO_2 coating were subsequently employed to enhance the acid strength and erase the undesirable external acid sites, respectively. Benefiting from the multiple zeolite modification steps, the PX selectivity and STY were increased to 33.8% and 3.0 g_{CH2} h^{-1} $kgcat^{-1}$, respectively, via the bifunctional catalyst Cr_2O_3/C&Cu-ZSM-5^T@SiO_2. With the aid of catalyst characterization, it is concluded that the dominant sinusoidal channel openings and external acid site suppression guaranteed the increased PX selectivity. At the same time, the enhanced acid strength stems from Cu ion doping and could increase the CO_2 conversion by facilitating the consumption of key reaction intermediates and strengthening the driving force in the tandem process. We anticipate that the comprehensive strategy proposed in this work could guide the rational

design of bifunctional catalysts for the oriented conversion of CO_2 + H_2 or syngas into the targeted product.

Author Contributions: Conceptualization, S.L. and Y.W.; methodology, S.L. and R.H.; validation, S.L., W.W. and Y.G.; formal analysis, S.L., R.H., W.W. and Q.L.; investigation, S.L. and R.H.; resources, Y.W. and M.W.; writing—original draft preparation, S.L.; writing—review and editing, Y.W. and M.W.; visualization, S.L., R.H., W.W. and Y.G.; supervision, Y.W. and M.W.; project administration, Y.W. and M.W. All authors have read and agreed to the published version of the manuscript.

Funding: This research was funded by the National Natural Science Foundation of China (22108310), the Shandong Province Key Research Program (Major Scientific and Technological Innovation Project, 2020CXGC010402), the Science and Technology Innovation Project of the Shandong Energy Group Co., Ltd. (SNKJ2021BJ04, SNKJ2023A03), the CNPC Innovation Foundation (2020D-5007-0407), and the Foundation of State Key Laboratory of High-Efficiency Utilization of Coal and Green Chemical Engineering (2022-K-75).

Data Availability Statement: The data presented in this study are available on request from the corresponding author.

Conflicts of Interest: The authors declare no conflict of interest.

References

1. Ding, M.; Flaig, R.W.; Jiang, H.-L.; Yaghi, O.M. Carbon capture and conversion using metal–organic frameworks and MOF-based materials. *Chem. Soc. Rev.* **2019**, *48*, 2783–2828. [CrossRef]
2. Feldman, D.R.; Collins, W.D.; Gero, P.J.; Torn, M.S.; Mlawer, E.J.; Shippert, T.R. Observational determination of surface radiative forcing by CO_2 from 2000 to 2010. *Nature* **2015**, *519*, 339–343. [CrossRef]
3. Keith, D.W. Why capture CO_2 from the atmosphere? *Science* **2009**, *325*, 1654–1655. [CrossRef]
4. Zhou, W.; Cheng, K.; Kang, J.; Zhou, C.; Subramanian, V.; Zhang, Q.; Wang, Y. New horizon in C1 chemistry: Breaking the selectivity limitation in transformation of syngas and hydrogenation of CO_2 into hydrocarbon chemicals and fuels. *Chem. Soc. Rev.* **2019**, *48*, 3193–3228. [CrossRef]
5. Wang, W.-H.; Himeda, Y.; Muckerman, J.T.; Manbeck, G.F.; Fujita, E. CO_2 hydrogenation to formate and methanol as an alternative to photo- and electrochemical CO_2 reduction. *Chem. Rev.* **2015**, *115*, 12936–12973. [CrossRef]
6. Wei, J.; Yao, R.; Han, Y.; Ge, Q.; Sun, J. Towards the development of the emerging process of CO_2 heterogenous hydrogenation into high-value unsaturated heavy hydrocarbons. *Chem. Soc. Rev.* **2021**, *50*, 10764–10805. [CrossRef]
7. Lyons, T.W.; Guironnet, D.; Findlater, M.; Brookhart, M. Synthesis of *p*-Xylene from ethylene. *J. Am. Chem. Soc.* **2012**, *134*, 15708–15711. [CrossRef]
8. Tsubaki, N.; Wang, Y.; Yang, G.; He, Y. Rational design of novel reaction pathways and tailor-made catalysts for value-added chemicals synthesis from CO_2 hydrogenation. *Bull. Chem. Soc. Jpn.* **2023**, *96*, 291–302. [CrossRef]
9. Wang, Y.; Gao, X.; Wu, M.; Tsubaki, N.J.E. Thermocatalytic hydrogenation of CO_2 into aromatics by tailor-made catalysts: Recent advancements and perspectives. *EcoMat.* **2021**, *3*, e12080. [CrossRef]
10. Tian, G.; Zhang, C.; Wei, F. CO_x conversion to aromatics: A mini-review of nanoscale performance. *Nanoscale Horiz.* **2022**, *7*, 1478–1487. [CrossRef]
11. Wang, D.; Xie, Z.H.; Porosoff, M.; Chen, J.G. Recent advances in carbon dioxide hydrogenation to produce olefins and aromatics. *Chem* **2021**, *7*, 2277–2311. [CrossRef]
12. Song, G.; Li, M.; Yan, P.; Nawaz, M.A.; Liu, D. High conversion to aromatics via CO_2-FT over a CO-reduced Cu-Fe_2O_3 Catalyst integrated with HZSM-5. *ACS Catal.* **2020**, *10*, 11268–11279. [CrossRef]
13. Wang, Y.; Kazumi, S.; Gao, W.; Gao, X.; Li, H.; Guo, X.; Yoneyama, Y.; Yang, G.; Tsubaki, N. Direct conversion of CO_2 to aromatics with high yield via a modified Fischer-Tropsch synthesis pathway. *Appl. Catal. B Environ.* **2020**, *269*, 118792. [CrossRef]
14. Cui, X.; Gao, P.; Li, S.; Yang, C.; Liu, Z.; Wang, H.; Zhong, L.; Sun, Y. Selective production of aromatics directly from carbon dioxide hydrogenation. *ACS Catal.* **2019**, *9*, 3866–3876. [CrossRef]
15. Xu, Y.; Shi, C.; Liu, B.; Wang, T.; Zheng, J.; Li, W.; Liu, D.; Liu, X. Technology. Selective production of aromatics from CO_2. *Catal. Sci. Technol.* **2019**, *9*, 593–610. [CrossRef]
16. Wei, J.; Yao, R.; Ge, Q.; Xu, D.; Fang, C.; Zhang, J.; Xu, H.; Sun, J. Precisely regulating Bronsted acid sites to promote the synthesis of light aromatics via CO_2 hydrogenation. *Appl. Catal. B. Environ.* **2021**, *283*, 119648. [CrossRef]
17. Wang, Y.; Tan, L.; Tan, M.; Zhang, P.; Fang, Y.; Yoneyama, Y.; Yang, G.; Tsubaki, N. Rationally designing bifunctional catalysts as an efficient strategy to boost CO_2 hydrogenation producing value-added aromatics. *ACS Catal.* **2019**, *9*, 895–901. [CrossRef]
18. Zhang, J.; Zhang, M.; Chen, S.; Wang, X.; Zhou, Z.; Wu, Y.; Zhang, T.; Yang, G.; Han, Y.; Tan, Y. Hydrogenation of CO_2 into aromatics over a ZnCrOx–zeolite composite catalyst. *Chem. Commun.* **2019**, *55*, 973–976. [CrossRef]
19. Zhou, C.; Shi, J.; Zhou, W.; Cheng, K.; Zhang, Q.; Kang, J.; Wang, Y. Highly active ZnO-ZrO_2 aerogels integrated with H-ZSM-5 for aromatics synthesis from carbon dioxide. *ACS Catal.* **2020**, *10*, 302–310. [CrossRef]

20. Ni, Y.; Chen, Z.; Fu, Y.; Liu, Y.; Zhu, W.; Liu, Z. Selective conversion of CO_2 and H_2 into aromatics. *Nat. Commun.* **2018**, *9*, 3457. [CrossRef]
21. Wang, Y.; Gao, W.; Kazumi, S.; Li, H.; Yang, G.; Tsubaki, N. Direct and oriented conversion of CO_2 into value-added aromatics. *Chem. Eur. J.* **2019**, *25*, 5149–5153. [CrossRef] [PubMed]
22. Li, Z.; Qu, Y.; Wang, J.; Liu, H.; Li, M.; Miao, S.; Li, C. Highly selective conversion of carbon dioxide to aromatics over tandem catalysts. *Joule* **2019**, *3*, 570–583. [CrossRef]
23. Liu, Y.; Qiang, W.; Ji, T.; Zhang, M.; Li, M.; Lu, J.; Lu, Y. Uniform hierarchical MFI nanosheets prepared via anisotropic etching for solution-based sub–100-nm-thick oriented MFI layer fabrication. *Sci. Adv.* **2020**, *6*, eaay5993. [CrossRef]
24. Dai, W.; Kouvatas, C.; Tai, W.; Wu, G.; Guan, N.; Li, L.; Valtchev, V. Platelike MFI crystals with controlled crystal faces aspect ratio. *J. Am. Chem. Soc.* **2021**, *143*, 1993–2004. [CrossRef]
25. Chen, N.Y.; Kaeding, W.W.; Dwyer, F.G. Para-directed aromatic reactions over shape-selective molecular sieve zeolite catalysts. *J. Am. Chem. Soc.* **1979**, *101*, 6783–6784. [CrossRef]
26. Cheng, Y.-T.; Wang, Z.; Gilbert, C.J.; Fan, W.; Huber, G.W. Production of p-Xylene from biomass by catalytic fast pyrolysis using ZSM-5 catalysts with reduced pore openings. *Angew. Chem.* **2012**, *124*, 11259–11262. [CrossRef]
27. Vu, D.V.; Miyamoto, M.; Nishiyama, N.; Egashira, Y.; Ueyama, K. Selective formation of para-xylene over H-ZSM-5 coated with polycrystalline silicalite crystals. *J. Catal.* **2006**, *243*, 389–394. [CrossRef]
28. Miyake, K.; Hirota, Y.; Ono, K.; Uchida, Y.; Tanaka, S.; Nishiyama, N. Direct and selective conversion of methanol to para-xylene over Zn ion doped ZSM-5/silicalite-1 core-shell zeolite catalyst. *J. Catal.* **2016**, *342*, 63–66. [CrossRef]
29. Zhang, J.; Qian, W.; Kong, C.; Wei, F. Increasing para-Xylene selectivity in making aromatics from methanol with a surface-modified Zn/P/ZSM-5 catalyst. *ACS Catal.* **2015**, *5*, 2982–2988. [CrossRef]
30. Lu, P.; Fei, Z.; Li, L.; Feng, X.; Ji, W.; Ding, W.; Chen, Y.; Yang, W.; Xie, Z. Effects of controlled SiO_2 deposition and phosphorus and nickel doping on surface acidity and diffusivity of medium and small sized HZSM-5 for para-selective alkylation of toluene by methanol. *Appl. Catal. A Gen.* **2013**, *453*, 302–309. [CrossRef]
31. Zhang, P.; Tan, L.; Yang, G.; Tsubaki, N. One-pass selective conversion of syngas to para-xylene. *Chem. Sci.* **2017**, *8*, 7941–7946. [CrossRef]
32. Gao, W.; Guo, L.; Wu, Q.; Wang, C.; Guo, X.; He, Y.; Zhang, P.; Yang, G.; Liu, G.; Wu, J.; et al. Capsule-like zeolite catalyst fabricated by solvent-free strategy for para-Xylene formation from CO_2 hydrogenation. *Appl. Catal. B Environ.* **2022**, *303*, 120906. [CrossRef]
33. Wang, C.; Zhang, L.; Huang, X.; Zhu, Y.; Li, G.; Gu, Q.; Chen, J.; Ma, L.; Li, X.; He, Q.; et al. Maximizing sinusoidal channels of HZSM-5 for high shape-selectivity to p-xylene. *Nat. Commun.* **2019**, *10*, 4348. [CrossRef]
34. Gao, W.; Guo, L.; Cui, Y.; Yang, G.; He, Y.; Zeng, C.; Taguchi, A.; Abe, T.; Ma, Q.; Yoneyama, Y.; et al. Selective conversion of CO_2 into para-Xylene over a $ZnCr_2O_4$-ZSM-5 catalyst. *ChemSusChem* **2020**, *13*, 6541–6545. [CrossRef] [PubMed]
35. Wang, T.; Yang, C.; Gao, P.; Zhou, S.; Li, S.; Wang, H.; Sun, Y. ZnZrOx integrated with chain-like nanocrystal HZSM-5 as efficient catalysts for aromatics synthesis from CO_2 hydrogenation. *Appl. Catal. B Environ.* **2021**, *286*, 119929. [CrossRef]
36. Wang, Y.; Gao, W.; Wang, K.; Gao, X.; Zhang, B.; Zhao, H.; Ma, Q.; Zhang, P.; Yang, G.; Wu, M.; et al. Boosting the synthesis of value-added aromatics directly from syngas via a Cr_2O_3 and Ga doped zeolite capsule catalyst. *Chem. Sci.* **2021**, *12*, 7786–7792. [CrossRef]
37. Yang, Z.X.; Xia, Y.D.; Mokaya, R. Zeolite ZSM-5 with unique supermicropores synthesized using mesoporous carbon as a template. *Adv. Mater.* **2004**, *16*, 727–732. [CrossRef]
38. Wang, W.; He, R.; Wang, Y.; Li, M.; Liu, J.; Liang, J.; Yasuda, S.; Liu, Q.; Wu, M.; Tsubaki, N. Boosting methanol-mediated CO_2 hydrogenation into aromatics by synergistically tailoring oxygen vacancy and acid site properties of multifunctional catalyst. *Chem. A Eur. J.* **2023**, e202301135. [CrossRef]

Disclaimer/Publisher's Note: The statements, opinions and data contained in all publications are solely those of the individual author(s) and contributor(s) and not of MDPI and/or the editor(s). MDPI and/or the editor(s) disclaim responsibility for any injury to people or property resulting from any ideas, methods, instructions or products referred to in the content.